XMM-Newton X-ray Detection of the High Magnetic Field Radio Pulsar PSR B1916+14

Weiwei Zhu[1], Victoria M. Kaspi[1,2], Marjorie E. Gonzalez[3], Andrew G. Lyne[4]

ABSTRACT

Using observations made with the *XMM-Newton* Observatory, we report the first X-ray detection of the high magnetic field radio pulsar PSR B1916+14. We show that the X-ray spectrum of the pulsar can be well fitted with an absorbed blackbody with temperature in the range of 0.08-0.23 keV, or a neutron star hydrogen atmosphere model with best-fit effective temperature of $\sim$0.10 keV, higher than expected from fast cooling models. The origin of the likely thermal emission is not well constrained by our short observation and is consistent with initial cooling or return-current heating. We found no pulsations in these data and set a 1σ upper limit on the pulsed fraction in the 0.1–2 keV band of $\sim$0.7. Implications of these results for our understanding of the different observational properties of isolated neutron stars are discussed.

Subject headings: pulsars: individual (PSR B1916+14) — X-rays: stars — stars: neutron

1. Introduction

In the past few decades, the boom in X-ray/gamma-ray astronomy has led to the discoveries of at least two new classes of isolated neutron star: magnetars and dim thermal isolated neutron stars (DTINS). These new classes exhibit distinctive properties different from those of conventional rotation-powered pulsars, the only kind of isolated neutron star known before. Magnetars, including anomalous X-ray pulsars (AXPs) and soft gamma-ray repeaters

[1]Department of Physics, McGill University, Montreal, QC, H3A 2T8, Canada; zhuww@physics.mcgill.ca, vkaspi@physics.mcgill.ca

[2]Canada Research Chair; Lorne Trottier Chair; R. Howard Webster Fellow of CIFAR

[3]Department of Physics and Astronomy, University of British Columbia, 6224 Agricultural Road Vancouver, BC, V6T 1Z1 Canada;

[3]University of Manchester, Jodrell Bank Observatory, Macclesfield, Cheshire, SK11 9DL, UK.

(SGRs), are slowly rotating neutron stars. They often emit luminously in the X-ray band and sometimes show dramatic outbursts and variability. Their X-ray emission and bursting activity are believed to be powered by enormous internal magnetic fields (10^{14}–10^{15} G; for reviews, see Woods & Thompson 2006; Kaspi 2007; Mereghetti 2008). The DTINS are nearby X-ray pulsars, having quasi-thermal spectra and no radio emission. They also appear to be slow rotators and are highly magnetized ($B \sim 10^{13}$ G; Kaplan & van Kerkwijk 2005; Zane et al. 2005; van Kerkwijk & Kaplan 2008; Kaplan & van Kerkwijk 2009). The nature and origin of these DTINS are still mysteries. A third possible new class is the so-called "Central Compact Object" (CCOs, De Luca et al. 2008; Pavlov & Luna 2009), apparently isolated neutron stars located in supernova remnants. However, it is not yet clear whether these are a truly distinct class as some CCOs have been recently revealed to be conventional rotation-powered pulsars (albeit with surprisingly low B fields; e.g. the CCO 1E1207.4−5209, Gotthelf & Halpern 2007).

What drives the different behaviors of these neutron stars? For magnetars, the answer is almost certainly their enormous magnetic field. Interestingly, the DTINS also appear to have higher magnetic fields than those of ordinary pulsars. Hence, it is sensible to suspect that magnetic field could be the primary defining characteristic of the three categories of isolated neutron stars. Based on the study of a large sample of isolated neutron stars, which includes most magnetars, some DTINS, and many ordinary radio pulsars, Pons et al. (2007) reported an intriguing correlation between the pulsar's blackbody temperature T, determined from the X-ray spectrum, and the magnetic field B, inferred from the spin-down ($T \propto B^{1/2}$). They also suggested that this correlation could be explained if the crusts of neutron stars were heated by magnetic-field decay, since it would significantly delay the cooling, particularly if the field were stronger than 10^{13} G. A similar correlation was also expected if the core of the neutron star is heated by magnetic field decay, with heat transfer out to the surface, leading to an increase of the surface temperature (Arras et al. 2004). Aguilera et al. (2008) expanded the work of Pons et al. (2007) through 2D cooling simulations that included anisotropic thermal conductivity and all relevant neutrino emission processes for realistic neutron stars, in an attempt to unite magnetar and DTINS in a simple picture of heating by magnetic field. Their study shows that the DTINS could be explained if they are old neutron stars ($\sim 10^6$ yr) born with 10^{14}–10^{15} G magnetic fields, or if they are middle-aged neutron stars born with 10^{13}–10^{14} G magnetic fields. This theory predicts that pulsars with magnetic field higher than 10^{13} G should be hotter than is predicted by a simple cooling model with lower magnetic field, regardless of whether they are radio-quiet or not. Therefore, observing high magnetic field radio pulsars at X-ray energies and measuring the temperature of their thermal radiation may help us unify the different classes of isolated neutron stars.

PSR B1916+14 is a radio pulsar having period P =1.181 s, with spin-down-inferred

magnetic field $B \equiv 3.2 \times 10^{19}(P\dot{P})^{1/2}$ G$= 1.6 \times 10^{13}$ G, spin-down age $\tau \equiv P/(2\dot{P}) = 8.8 \times 10^4$ yr, and $\dot{E} \equiv 4\pi^2 I\dot{P}/P^3 = 5 \times 10^{33}$erg s^{-1} (Hulse & Taylor 1974; Manchester et al. 2005). It is a relatively young pulsar. Given its age, PSR B1916+14 should still be hot enough to be X-ray detectable, according to a minimal pulsar cooling model, without magnetic-field-decay heating (Page et al. 2006). It is also one of the highest-magnetic-field radio pulsars known and may therefore be hotter because of magnetic-field decay. This makes PSR B1916+14 a good test subject for neutron star cooling models, and hence X-ray observations.

2. Observations and Results

PSR B1916+14 was observed by the *Newton X-ray Multi-Mirror Mission* (*XMM*) observatory (Jansen et al. 2001) on 2008 March 25. Both the European Photon Imaging Camera (EPIC) pn (Strüder et al. 2001) camera and the EPIC MOS cameras (Turner et al. 2001) were operating in full window mode with the thin filter, and with a pointing offset of $1'.107$. We analyzed the data taken in this *XMM* observation, and found that PSR B1916+14 was clearly detected in both the pn and MOS data.

2.1. Imaging and Source Detection

The *XMM* data were analyzed with the *XMM* Science Analysis System (SAS) version 8.0.0[1] and the latest calibrations (updated 2008 Oct 3). To exclude strong background flares that sometimes contaminate *XMM* data, we extracted light curves of photons above 10 keV from the entire field-of-view of the pn and MOS images, and excluded the time intervals in which background flares occurred for all subsequent analyses. The total exposure time of the observation is ~ 25 ks. However, after excluding the bad time intervals within which the background flux was very high (>10 counts per second) and showing significant burst-like features, only 12 ks of pn, 11 ks of MOS1 and 13 ks of MOS2 data were used in our analysis. The data were also corrected to the barycenter using the SAS `barycen` tool after background flares were excluded, using the nominal pulsar position (J2000) RA 19:18:23.638(7) DEC +14:45:06.00(15) (Hobbs et al. 2004).

In order to find the X-ray counterpart of PSR B1916+14 , we used the SAS tool `edetect_chain` to perform a blind search for point sources. `edetect_chain` is designed to find point sources using a sliding cell technique and to calculate the significance of any

[1]See http://xmm.esac.esa.int/sas/8.0.0/

detection using a maximum likelihood method. It generates an output source list file containing information like total counts, position and significance of detected sources. In the pn image, a point source was detected coincident with the position of PSR B1916+14 (Fig. 1) by `edetect_chain`. The source has 133 ± 15[2] counts in 0.1–10 keV band and a likelihood ratio of $L_2 = -\ln(P) \simeq 143$ (where P is the probability for a random Poissonian fluctuation to have caused the observed source counts). This source was also detected in the MOS 1 image with 22 ± 7 counts and $L_2 \simeq 11$, and in the MOS 2 images with 46 ± 9 counts and $L_2 \simeq 48$, both in the 0.1–10 keV range. Thus, this point source was clearly detected in the pn and the MOS data.

Figure 1 is the pn image, smoothed with a Gaussian profile of radius $\sigma = 8''.2$. The small circle in the center of the image marks the radio position of PSR B1916+14 . The position uncertainty is smaller than the size of the circle (Hobbs et al. 2004). The best-fit position of the detected source given by `edetect_chain` is (J2000) RA 19:18:23.74(5) DEC +14:45:06.2(8), consistent with the radio position of PSR B1916+14 . Therefore, it is very likely that the source we detected is the X-ray counterpart of PSR B1916+14 .

The radially averaged profile of *XMM* 's point spread function can be approximated by an analytic function – the King function $\rho(r) = A[1 + (\frac{r}{r_0})^2]^{-\alpha}$, where $\rho(r)$ is the number density of counts at radius r, A is a normalization parameter, r is the radial distance between the events and the center of the source, r_0 and α are parameters reflecting the size and shape of the point spread function (PSF) and are functions of energy and off-axis angle.[3] In order to search for evidence of extended emission from PSR B1916+14 , we extracted 0.2-12 keV photon events from a circular region of $35''$ radius around the best-fit position, and calculated the radial distance between every photon event and the pulsar, to get the radially averaged profile. Using the Kolmogorov-Smirnov (K-S) test, we then compared the observed radially averaged profile to a model composed of a King function. Given the small off-axis angle, and the energy distribution of the source, we chose $\alpha = 1.6$ and $r_0 = 5.25$ pixels$= 21''.525$ and a uniform background (0.05 photons/acrsec^2, inferred from the 397 photons found in a circular background region of $50''$ radius and $\sim 3'$ away from PSR B1916+14). The K-S test shows that the radially averaged profile can be well matched by the specified King function. Therefore, there is no evidence for extended emission near PSR B1916+14 from this observation.

---

[2]Unless otherwise specified, the uncertainties quoted in this paper represent a 1σ range.

[3]See http://xmm.esac.esa.int/docs/documents/CAL-TN-0018-2-6.pdf, page 6

2.2. Spectroscopy

We extracted the X-ray spectrum of PSR B1916+14 from the pn data using a circular region of 32″.5 radius encircling the source. The source region should contain more than 80% of the counts from a point source. The background spectrum was extracted from a circular region of 50″ radius and ∼3′ away from the pulsar where no source was detected. Both single- and double- events were selected, but events that hit or were close to a bad pixel or CCD gap were excluded using the filter expression FLAG = 0&&PATTERN <= 4. A response file and an auxiliary response file were generated using the SAS command `rmfgen` and `arfgen`. The spectrum was grouped to have a minimum of 15 photons per bin using the `ftool grppha`, and was then fed to XSPEC 12.3.0[4] for spectral fitting.

We also extracted spectra from the data of the two MOS detectors using source circular regions of 36″ radius and background regions of ∼ 60″ radius. Single- to quadruple- photon events were selected except those that landed on a bad pixel or CCD gap, using the filter expression of XMMEA_EM&&PATTERN <= 12. We then combined the two MOS spectra into a single MOS spectrum and averaged their background, response and auxiliary files using the `ftool addspec`. The resulting MOS spectrum was also grouped to have a minimum of 15 photons per bin and was fitted jointly with the pn spectrum.

The X-ray spectra of PSR B1916+14 can be well fit with an absorbed blackbody model. However, due to the small number of counts, the column density N_H was poorly constrained. The best-fit N_H is $\sim 1 \times 10^{19}$ cm^{-2}, too small given the estimated distance and location of the pulsar. Therefore, we estimated the N_H for this pulsar based on the total N_H (1.58×10^{22} cm^{-2}) of the Galaxy along the line-of-sight[5] and the distance to the pulsar (2.1 ± 0.3 kpc, estimated from the 27.2 pc cm^{-3} dispersion measure of the pulsar; Cordes & Lazio 2002), and find a moderate value of $\sim 0.14 \times 10^{22}$ cm^{-2}. Fixing N_H to this value, the best-fit blackbody temperature for the 0.1–2 keV spectra (Fig. 2) is 0.13 ± 0.01 keV (Table 1). The model-predicted absorbed flux in the 0.1–2 keV range is $1.4\pm0.3\times10^{-14}$ ergs s^{-1} cm^{-2}. Assuming a distance of 2.1 kpc, we find the bolometric X-ray luminosity of PSR B1916+14 to be $\sim 3 \times 10^{31}$ ergs s^{-1}.

By fixing N_H while fitting the pn and MOS spectra, we underestimate the uncertainties of the best-fit parameters. In order to get a sense of the real uncertainty of kT, we tried fitting with a range of N_H. N_H likely lies between 0.07×10^{22} cm^{-2} and 0.3×10^{22} cm^{-2}. It is probably not smaller than 0.07×10^{22} cm^{-2} because the distance estimated from the dispersion measure

[4]http://heasarc.gsfc.nasa.gov/docs/xanadu/xspec/

[5]http://cxc.harvard.edu/toolkit/colden.jsp

is unlikely to be incorrect by more than 50%. Also, an absorbed blackbody model with N_H higher than 0.3×10^{22} cm^{-2} cannot fit the spectra well for any kT. With N_H restricted to lie between these two values, the acceptable (null hypothesis possibility of the fit > 0.01) range of kT is 0.08 to 0.23 keV (with blackbody radius range from ∼6 km to ∼0.2 km). This temperature range reflects reasonable uncertainties on N_H, and is quoted in the abstract and Figures 3 and 4 (see below).

The pn and MOS spectra could also be fit with a power-law model, with a best-fit N_H of $0.12^{+0.05}_{-0.07} \times 10^{22}$ cm^{-2} and a photon index of Γ $\sim 3.5^{+1.6}_{-0.7}$ (Table 1). The lack of source photons with energy above 2 keV results in a soft best-fit power-law model. This is rarely seen from other non-thermally emitting pulsars. Therefore, it is very unlikely that the X-ray emission of PSR B1916+14 is non-thermal.

A neutron-star hydrogen atmosphere (NSA) model (with magnetic field strength set to 10^{13} G; Zavlin et al. 1996; Pavlov et al. 1995) could also fit the pn and MOS spectra. However, the parameters are even less constrained in comparison with the blackbody model. We had to freeze the mass of the neutron star to 1.4 $M_\odot$ and the distance to 2.1 kpc to get a better-constrained fit ($\chi^2(\nu) = 14.3(17)$). The best-fit N_H is $0.23^{+0.09}_{-0.04} \times 10^{22}$cm^{-2}, kT is 0.10 ± 0.04 keV, and the resulting best-fit neutron-star radius is ∼6 km. Unfortunately, the radius is not well constrained in this model and has a 1σ upper limit of 20 km. The model predicted 0.1–2 keV X-ray luminosity is $(7 \pm 4) \times 10^{31}$ergs s^{-1}.

2.3. Timing analysis

To search for X-ray pulsations from PSR B1916+14 , we folded all the pn source events from a total 25 ks exposure without filtering for the background flares using 16 phase bins and a contemporaneous ephemeris which was derived from radio timing data obtained using the 76-m telescope at the Jodrell Bank Observatory (Hobbs et al. 2004). The MOS full-window mode data is useless for timing analysis because of its 2.7 s time resolution. A total of 374 pn photon events were extracted without filtering for background flares, all in the range of 0.1-2 keV, from a source region of 15″ radius chosen to reduce the number of background photons and improve the signal-to-noise ratio. From the same energy band and the same CCD, 1945 events were found in a circular background region of 50″ radius where no source was detected by the SAS tool `edetect_chain`. If the background is uniformly distributed, there should be 175±4 background photons in the source region. The folded and binned light curve was fit to a constant line. The best-fit χ^2 was 9.6 for 15 degrees of freedom. Therefore no significant pulsations were detected.

In order to determine an upper limit on the pulsed fraction, we simulated event lists with the same total number of counts as in the observed event list. The simulated event lists were generated assuming the signal has a sinusoidal profile starting at a random phase and a specified area pulsed fraction, where the area pulsed fraction is defined as the ratio of the pulsed part of profile to the entire profile. For a sinusoidal profile $F = A\sin\theta + B$, where F is the count rate, A is the amplitude, B is the DC level, and θ is the phase, the area pulsed fraction is $A/(2B + A)$. By specifying different area pulsed fractions, we found that, if we set the area pulsed fraction of the simulated event lists to 35%, then approximately 68% of them would be detected with $> 3\sigma$ significance. Because there are ∼175 background photons in the 374 photons from the source region, the 1σ area pulsed fraction upper limit of the pulsar is ~ 0.7. This is not an especially interesting constraint because the number of source photons was so small that even a highly pulsed signal could have gone undetected.

3. Discussion

The X-ray spectrum of PSR B1916+14 is soft, and therefore is most likely thermal. The blackbody temperature lies in the range of 0.08–0.23 keV, and the best-fit effective temperature of NSA model is 0.10±0.04 keV. Given PSR B1916+14 's age, its temperature is consistent with what one would expect ($kT \sim 0.07$–0.11 keV) from minimal cooling models in which magnetic field is not considered (Page et al. 2006). Its estimated bolometric luminosity ($\sim 3 \times 10^{31}$erg s^{-1}; Table 1) is somewhat low when compared with the curves of Page et al. (2006), suggesting that the pulsar may have a light-element envelope. However the substantial uncertainties on the luminosity preclude a firm conclusion. On the other hand, fast cooling models predict much lower temperatures ($kT < 30$ eV; e.g. Yakovlev & Pethick 2004) which would be undetectable with current instruments. Therefore, fast cooling seems unlikely for PSR B1916+14 from our observation.

The small best-fit blackbody radius (0.8±0.1 km; Table 1) suggests polar-cap reheating. If the emission of the pulsar is due to curvature radiation, return-current heating is predicted to give rise to an X-ray luminosity (see Harding & Muslimov 2001 and Eq. 7.2 in Kaspi et al. 2006 for details)

$$L_+^{(CR)} \simeq 10^{31}\mathrm{erg\ s^{-1}} \begin{cases} 0.4P^{-6/7}(\tau/10^6)^{-1/7} & \text{if } P \le 0.1(B/10^{12})^{4/9} \\ 1.0P^{-1/2} & \text{if } P \ge 0.1(B/10^{12})^{4/9}, \end{cases} \quad (1)$$

where τ is in yr, P is in s, and B is in G. For PSR B1916+14 , $L_+^{(CR)}$ is $\sim 9\times10^{30}$erg s^{-1}, only a factor of ∼3 smaller than the estimated blackbody bolometric luminosity (see Table 1). If the emission is due to inverse Compton scattering, the return current heating will be much less

effective (Harding & Muslimov 2002). Given that the best-fit blackbody parameters are not well constrained, we cannot rule out return current heating as the origin of PSR B1916+14 's X-ray luminosity. We note that the NSA model (Section 2.2) yields a larger radius, although it is also not well constrained.

To compare the properties of PSR B1916+14 to those of other X-ray-detected radio pulsars, we have collected the temperature, magnetic field strength, and spin-down energy of a dozen such pulsars from the literature, and listed them in Table 2. For pulsars in this Table, we also made plots of their temperature versus age and magnetic field (Figs. 3 and 4, respectively). Given the large uncertainty on the temperature measurement from our short-exposure observation of PSR B1916+14 , we cannot conclude here whether thermal emission is consistent with minimal cooling or if the neutron star is hotter than lower-magnetic-field pulsars of the same age, as expected in some models (Pons et al. 2007; Aguilera et al. 2008). A longer observation in the future may be able to distinguish among thermal models.

However, we note with interest that the previously published temperature of PSR J0538+2817 is surprisingly high, in spite of its relatively large age (40 kyr) and relatively low magnetic field (7.3×10^{11} G; Table 2). In contrast to PSR B1916+14 , PSR J0538+2817's emission is unlikely to be from polar-cap reheating because of the very high required efficiency for conversion of $\dot{E}$ to X-ray luminosity, $\sim 10^{-2}$, compared with the $\sim 5 \times 10^{-4}$ predicted by Equation 1 above for this pulsar. If correct, the high temperature suggests a wider range of possible temperatures for young neutron stars than is currently predicted. This would be a challenge to the Pons et al. (2007) model.

Although PSR B1916+14 is detected by *XMM* as a point source with no evidence of extended emission, it is still possible that extended emission was too faint to be detectable. Based upon the number of counts in the background region, we found that, in the 0.3–8 keV band, extended emission of surface brightness smaller than $\sim 3 \times 10^{-6}$ count $s^{-1}arcsec^{-2}$ would not be detected (with 3σ significance) in our observation. This limits our sensitivity for detecting a very faint pulsar wind nebula (PWN) like that of the Geminga pulsar, which has a surface brightness of $\sim 1 \times 10^{-6}$ count $s^{-1}arcsec^{-2}$ (Pavlov et al. 2006) in the same energy range, despite the fact that Geminga is closer by a factor of ∼8. Assuming there is an undetected PWN around PSR B1916+14 having a spectrum like that of the Geminga PWN (power law with index 1.0), we can estimate the upper limit of its surface brightness to be $\sim 3 \times 10^{-17}$ erg $cm^{-2}s^{-1}arcsec^{-2}$, in the 0.3–8 keV range. If we further assume that the PWN is uniformly distributed in a circular region of radius 20″, then this surface brightness upper limit corresponds to a PWN luminosity upper limit of $\sim 3 \times 10^{31}$ erg s^{-1}.

Geppert et al. (2004) showed that the presence of a very high magnetic field could cause inhomogeneous thermal conductivity in the neutron star crust and lead to the formation of

hot spots on the neutron star surface. It could also cause strong radiative beaming of the thermal emission from the neutron star. These effects could give rise to highly pulsed X-rays, as in the $74 \pm 14\%$ pulsed fraction observed from the high-magnetic-field radio pulsar PSR J1119−6127 (Gonzalez et al. 2005). However, limited by the exposure time of the observation, we did not detect any X-ray pulsations from PSR B1916+14 . Future longer observations will be useful for better constraining its pulsed fraction.

We thank S. Bogdanov and S. Guillot for useful comments. We thank the referee Craig Heinke for helpful suggestions. VMK is supported by an NSERC Discovery Grant, CIFAR, FQRNT, the Canada Research Chairs Program, and the McGill Lorne Trottier Chair.

REFERENCES

Aguilera, D. N., Pons, J. A., & Miralles, J. A. 2008, ApJ, 673, L167

Arras, P., Cumming, A., & Thompson, C. 2004, ApJ, 608, L49

Chevalier, R. A. 2005, ApJ, 619, 839

Cordes, J. M. & Lazio, T. J. W. 2002, astro-ph/0207156

De Luca, A., Caraveo, P. A., Mereghetti, S., Negroni, M., & Bignami, G. F. 2005, ApJ, 623, 1051

De Luca, A., Mignani, R. P., Zaggia, S., Beccari, G., Mereghetti, S., Caraveo, P. A., & Bignami, G. F. 2008, ApJ, 682, 1185

Geppert, U., Küker, M., & Page, D. 2004, A&A, 426, 267

Gonzalez, M. E., Kaspi, V. M., Camilo, F., Gaensler, B. M., & Pivovaroff, M. J. 2005, ApJ, 630, 489

Gotthelf, E. V. & Halpern, J. P. 2007, ApJ, 664, L35

Gotthelf, E. V., Halpern, J. P., & Dodson, R. 2002, ApJ, 567, L125

Harding, A. K. & Muslimov, A. G. 2001, ApJ, 556, 987

—. 2002, ApJ, 568, 862

Hobbs, G., Lyne, A. G., Kramer, M., Martin, C. E., & Jordan, C. 2004, MNRAS, 353, 1311

Hulse, R. A. & Taylor, J. H. 1974, ApJ, 191, L59

Jackson, M. S. & Halpern, J. P. 2005, ApJ, 633, 1114

Jansen, F., Lumb, D., Altieri, B., Clavel, J., Ehle, M., Erd, C., Gabriel, C., Guainazzi, M., Gondoin, P., Much, R., Munoz, R., Santos, M., Schartel, N., Texier, D., & Vacanti, G. 2001, A&A, 365, L1

Kaplan, D. L. & van Kerkwijk, M. H. 2005, ApJ, 628, L45

Kaplan, D. L. & van Kerkwijk, M. H. 2009, ApJ, 692, L62

Kaspi, V. M. 2007, Ap&SS, 308, 1

Kaspi, V. M., Roberts, M. S. E., & Harding, A. K. 2006, in Compact Stellar X-ray Sources, ed. W. H. G. Lewin & M. van der Klis (UK: Cambridge University Press)

Manchester, R. N., Hobbs, G. B., Teoh, A., & Hobbs, M. 2005, VizieR Online Data Catalog, 7245, 0

Manzali, A., De Luca, A., & Caraveo, P. A. 2007, ApJ, 669, 570

McGowan, K. E., Kenea, J. A., Zane, S., Cordova, F. A., Cropper, M., Ho, C., Sasseen, T., & Vestrand, W. T. 2003, ApJ, 591, 380

McGowan, K. E., Zane, S., Cropper, M., Vestrand, W. T., & Ho, C. 2006, ApJ, 639, 377

Mereghetti, S. 2008, A&A Rev., 15, 225

Ng, C.-Y., Romani, R. W., Brisken, W. F., Chatterjee, S., & Kramer, M. 2007, ApJ, 654, 487

Page, D., Geppert, U., & Weber, F. 2006, Nuclear Physics A, 777, 497

Pavlov, G. G., Kargaltsev, O., & Brisken, W. F. 2008, ApJ, 675, 683

Pavlov, G. G. & Luna, G. J. M. 2009, astro-ph/0905.3190

Pavlov, G. G., Sanwal, D., & Zavlin, V. E. 2006, ApJ, 643, 1146

Pavlov, G. G., Shibanov, Y. A., Zavlin, V. E., & Meyer, R. D. 1995, in The Lives of the Neutron Stars (NATO ASI Series), ed. A. Alpar, Ü. Kiziloğlu, & J. van Paradis (Dordrecht: Kluwer), 71–90

Pons, J. A., Link, B., Miralles, J. A., & Geppert, U. 2007, Physical Review Letters, 98, 071101

Slane, P. 1994, ApJ, 437, 458

Slane, P., Helfand, D. J., van der Swaluw, E., & Murray, S. S. 2004, ApJ, 616, 403

Strüder, L., et al., 2001, A&A, 365, L18

Turner, M. J. L., et al., 2001, A&A, 365, L27

van Kerkwijk, M. H. & Kaplan, D. L. 2008, ApJ, 673, L163

Weisskopf, M. C., O'Dell, S. L., Paerels, F., Elsner, R. F., Becker, W., Tennant, A. F., & Schwarz, D. A. 2004, ApJ, 601, 1050

Woods, P. M. & Thompson, C. 2006, in Compact Stellar X-ray Sources, ed. W. H. G. Lewin & M. van der Klis (UK: Cambridge University Press)

Zane, S., Cropper, M., Turolla, R., Zampieri, L., Chieregato, M., Drake, J. J., & Treves, A. 2005, ApJ, 627, 397

Yakovlev, D. G. & Pethick, C. J. 2004, ARAA, 42, 169

Zavlin, V. E., Pavlov, G. G., & Shibanov, Y. A. 1996, A&A, 315, 141

Table 1. Best-fit Spectral Parameters for PSR B1916+14

Parameter	Blackbody model[a]	Power-law model	NSA model
N_H (10^{22} cm^{-2})	0.14	$0.12^{+0.05}_{-0.07}$	$0.23^{+0.09}_{-0.04}$
kT (keV)	0.13±0.01	—	0.10 ± 0.04
R_{bb} (km)	0.8 ± 0.1	—	—
R_{NS} (km)	—	—	∼6
Γ	—	$3.5^{+1.6}_{-0.7}$	—
χ^2(dof)	14.1(18)	13.9(17)	14.3(17)
$f_{\rm abs}$[b] (ergs s^{-1} cm^{-2})	1.4±0.3×10^{-14}	$1.7^{+0.4}_{-0.6}\times10^{-14}$	$(1.7\pm0.3) \times 10^{-14}$[d]
$f_{\rm unabs}$[c] (ergs s^{-1} cm^{-2})	$(5 \pm 1)\times10^{-14}$	$\sim 2\times10^{-13}$	$(1.4\pm0.8) \times 10^{-13}$[d]
$L_{\rm X}$ (ergs s^{-1})	$\sim 3\times10^{31}$[e]	$\sim 1\times10^{32}$[f]	$(7 \pm 4) \times 10^{31}$[d]

[a]Best-fit parameters of absorbed blackbody fit to the *XMM* spectra. N_H was frozen when fitting, so the uncertainties of the parameters, especially that of the kT, do not reflect the uncertainties on N_H; see text for details. Emission radius R_{bb} was inferred assuming a distance of 2.1 kpc (estimated from the dispersion measure; Hobbs et al. 2004).

[b]Absorbed X-ray flux, $f_{\rm abs}$ in the 0.1–2 keV range.

[c]Unabsorbed X-ray flux, $f_{\rm unabs}$, in the 0.1–2 keV range; the uncertainty was propagated from the uncertainties on the parameters and absorbed flux.

[d]When fitting with NSA model, the flux and luminosity are estimated using the `cflux` model in `xspec`.

[e]Bolometric X-ray luminosity derived assuming a distance of 2.1 kpc.

[f]Inferred X-ray luminosity in the 0.1–10 keV range assuming a distance of 2.1 kpc.

Table 2. Parameters of the X-ray-detected Radio Pulsars

Name	Age[a] (kyr)	kT[b] (eV)	B[c] (G)	$\dot{E}$[c] (erg s^{-1})	Observatory	Spectral model[d]	Reference
B1916+14	88	135(45)	1.6×10^{13}	5.1×10^{33}	*XMM*	BB	this work
B1055−52	540	68(3)	1.1×10^{12}	3.0×10^{34}	*XMM*	BB+BB+PL	De Luca et al. 2005
J0633+1746 (Geminga)	340	41.4(0.1)	1.6×10^{12}	3.2×10^{34}	*XMM*	BB+PL	Jackson & Halpern 2005
B0656+14	110	56.0(0.9)	4.7×10^{12}	3.8×10^{34}	*XMM*	BB+BB+PL	De Luca et al. 2005
B0355+54	562	82(4)	8.4×10^{11}	4.5×10^{34}	*ROSAT/Einstein*	BB	Slane 1994
J0538+2817	40[e]	183(3)	7.3×10^{11}	4.9×10^{34}	*XMM*	BB	McGowan et al. 2003
B2334+61	41	109(35)	9.9×10^{12}	6.2×10^{34}	*XMM*	BB+PL	McGowan et al. 2006
B1823−13	21	135(14)	2.3×10^{12}	2.8×10^{36}	*Chandra*	BB	Pavlov et al. 2008
B1706−44	17.4	143(14)	3.1×10^{12}	3.4×10^{36}	*Chandra*	BB+PL	Gotthelf et al. 2002
J1811−1925	2[f]	<150	1.7×10^{12}	6.4×10^{36}	*Chandra*	BB+PL	Kaspi et al. 2006
B0833−45 (Vela)	11	91(3)	3.4×10^{12}	6.9×10^{36}	*XMM*	BB+BB+PL	Manzali et al. 2007
J0205+6449	2.4[f]	112(9)	3.6×10^{12}	2.7×10^{37}	*Chandra*	BB+PL	Slane et al. 2004
B0531+21 (Crab)	0.955[f]	<172	3.8×10^{12}	4.6×10^{38}	*Chandra*	BB+PL	Weisskopf et al. 2004

[a]The spin-down age unless otherwise noted.

[b]The blackbody temperature or the temperature of the softer blackbody component as measured by fitting the data with different spectral models as listed in this Table.

[c]Numbers were found in the ATNF database (Manchester et al. 2005).

[d]BB: blackbody model; BB+PL: blackbody plus power-law model; BB+BB+PL: two blackbody plus power-law model.

[e]The age of PSR J0538+2817 estimated based on the proper motion of the pulsar from its associated supernova remnant (SNR) (Ng et al. 2007).

[f]The age of SNR with which the pulsar is associated, estimated based on its expansion rate: PSR J1811−1925 (Kaspi et al. 2006); PSR J0205+6449 (Chevalier 2005). The age of PSR B0531+21 (Crab pulsar) is based on historical record.

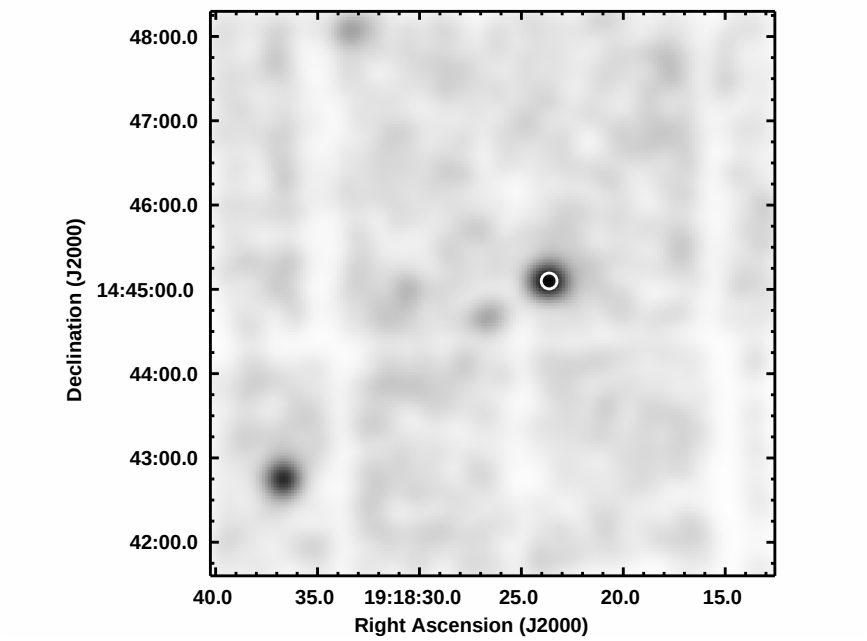

Fig. 1.— *XMM* image in the 0.2–2 keV energy band, smoothed by a Gaussian profile of 8.2″ radius (a profile that is slightly oversampling the telescope's PSF). The radio position of PSR B1916+14 is labeled by the white circle. Note that the radius of the circle is much larger than the uncertainty on the radio position.

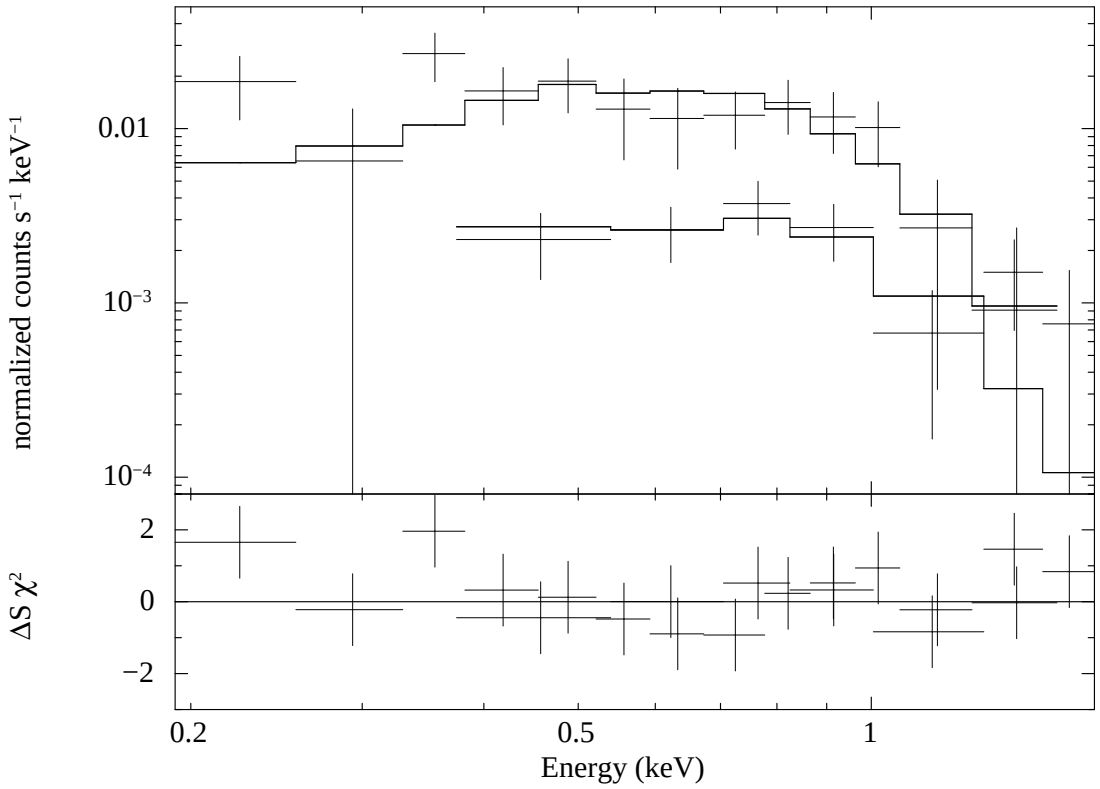

Fig. 2.— *XMM* spectra (upper is pn, lower is combined MOS) of PSR B1916+14 , with the best blackbody fit (see Table 1). The spectra are binned to contain a minimum of 15 counts per bin.

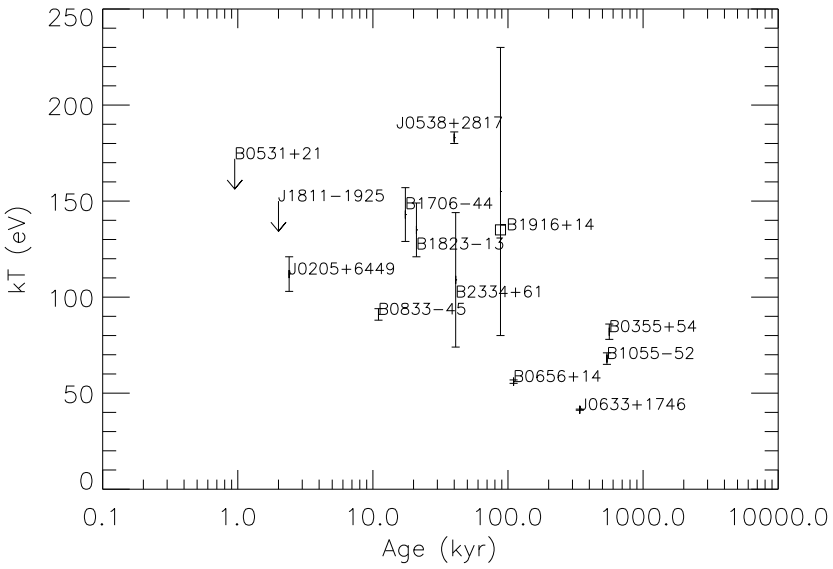

Fig. 3.— Observed temperature (kT) versus age for X-ray-detected radio pulsars. Note that for PSR B1916+14 we used the kT measured by allowing N_H to vary in a reasonable range; the same is not necessarily true for the other measurements; see original references for details.

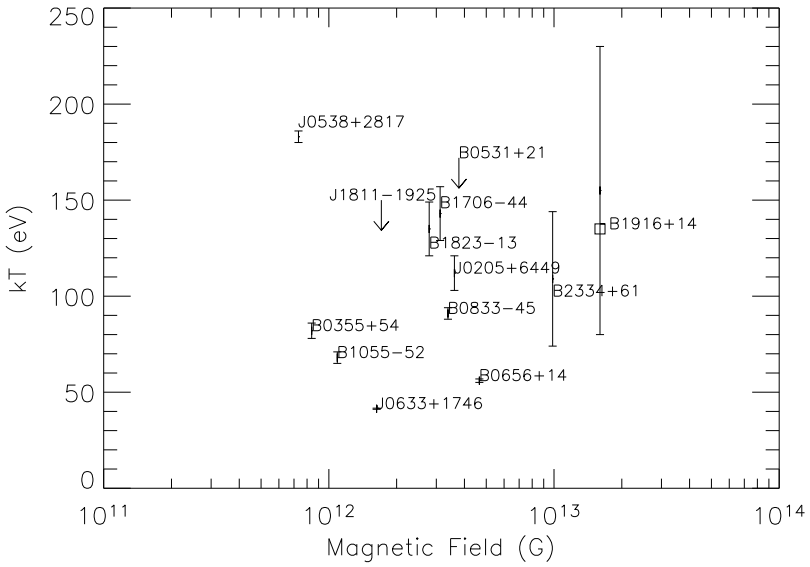

Fig. 4.— Observed temperature (kT) versus magnetic field strength for X-ray-detected radio pulsars. See caption for Figure 3 for caveats.